Matrix Infrared Spectra of the C−H Insertion and Dihydrido Cyclic Products from Reactions of Group 3 Metal Atoms with Ethylene

Han-Gook Cho and Lester Andrews*

Department of Chemistry, University of Incheon, 177 Dohwa-dong, Nam-ku, Incheon 402-749, South Korea, and Department of Chemistry, University of Virginia, P.O. Box 400319, Charlottesville, Virginia 22904-4319

Received: March 20, 2009; Revised Manuscript Received: April 28, 2009

Reactions of laser-ablated Group 3 metal atoms with ethylene isotopomers have been carried out, and the primary products have been identified in the matrix IR spectra. The insertion and dihydrido cyclic products ($HM-C_2H_3$ and $H_2M-C_2H_2$) are identified from the matrix IR spectra of Sc and Y, whereas only the insertion product is observed in the La spectra along with many lanthanium hydride absorptions. The observed metal hydride absorptions suggest that the H_2-elimination reaction becomes faster upon going down the group column, and the trend is also consistent with the energies of the H_2-elimination products relative to those of the dihydrido cyclic products. The present results support the conclusion that C−H insertion and following H migration from C to M are in fact general phenomena in reactions of early transition metals (Groups 3−6) and actinides with ethylene. The back-donation of electron-deficient Group 3 metals to the π-cyclic system of $H_2M-C_2H_2$ is evidently much weaker than that of the previously studied systems.

Introduction

H_2-elimination from ethylene with transition-metal atoms has been carefully investigated in previous reaction dynamics studies, and the proposed reaction paths for the metal systems have been theoretically examined as well.[1–5] While Group 4 metals, such as Zr, turn out to be most reactive, the reactions of Groups 3 and 5 metals are also studied.[2,4,5] The results are generally interpreted with the reaction path that H_2-elimination by transition-metal atoms proceeds in the order of M + ethylene → π-complex → metallacyclopropane → insertion product → dihydrido cyclic complex → $M-C_2H_2 + H_2$.[5] The first formed weak π-complex converts to the more strongly bound complex (metallacyclopropane), which then undergoes C−H insertion to form $HM-CHCH_2$, and later rearranges to a dihydrido cyclic product ($H_2M-C_2H_2$). H_2-elimination is believed to occur from the dihydrido complex, leaving a metal−acetylene complex.

The C−H(X) insertion and subsequent rearrangement of alkanes and haloalkanes as well as ethylene have recently been executed with many transition metals, including actinides.[6–14] As a result, C−H bond insertion by transition metals and following variation in molecular structure have open a new way for synthetic and coordination chemistry, allowing possibilities to prepare more desirable end products and to discover practical applications.[7,8] Moreover, the identified transient species provide invaluable information for details of the reaction path and insights to understand the key steps for numerous synthetic reactions and catalytic processes as well.[10–13]

Recently, the insertion and dihydrido cyclic complexes are identified in the matrix IR spectra from reactions of Groups 4−6 metals[10–13] and actinide (Th and U)[14] atoms with ethylene isotopomers, providing strong evidence supporting the suggested reaction path for H_2-elimination.[1–5] The unexpected trihydrido ethynyl complex (MH_3-CCH) is also generated in reactions of Group 4 metals[11] and actinides,[14] indicating that second H-migration occurs from C to M.[11] Metal hydride (MH_x) absorptions observed in the matrix spectra of Groups 4 and 5 metals are regarded as evidence for efficient H_2-elimination,[11,12] whereas they do not appear in the spectra of Group 6 and actinide

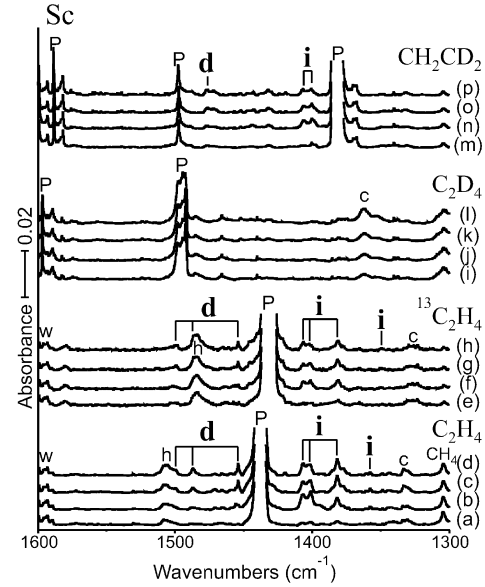

Figure 1. IR spectra in the region of 1600−1300 cm^{-1} for laser-ablated Sc atoms codeposited with ethylene isotopomers in excess argon at 10 K and their variation. (a) Sc + 0.5% C_2H_4 in Ar codeposited for 1 h. (b) As (a) after photolysis with $\lambda > 420$ nm. (c) As (b) after photolysis with $240 < \lambda < 380$ nm. (d) As (c) after annealing to 24 K. (e) Sc + 0.5% $^{13}C_2H_4$ in Ar codeposited for 1 h. (f) as (e) after photolysis with $\lambda > 420$ nm. (g) as (f) after photolysis with $240 < \lambda < 380$ nm. (h) as (g) after annealing to 24 K. (i) Sc + 0.5% C_2D_4 in Ar codeposited for 1 h. (j) as (i) after photolysis with $\lambda > 420$ nm. (k) as (j) after photolysis with $240 < \lambda < 380$ nm. (l) as (k) after annealing to 24 K. (m) Sc + 0.5% CH_2CD_2 in Ar codeposited for 1 h. (n) as (m) after photolysis with $\lambda > 420$ nm. (o) as (n) after photolysis with $240 < \lambda < 380$ nm. (p) as (o) after annealing to 24 K. The **i** and **d** denote the product absorption groups, c identifies product absorptions common to the precursor in other metal experiments, P designates unreacted precursor absorptions and w indicates water residue absorption.

* To whom correspondence should be addressed. E-mail: lsa@virginia.edu.

10.1021/jp9025464 CCC: $40.75
Published on Web 05/27/2009

TABLE 1: Frequencies of Product Absorptions Observed from Reactions of Sc with Ethylene in Excess Argon[a]

	C_2H_4	C_2D_4	$^{13}C_2H_4$	CH_2CD_2	description
d	1499.8, 1487.3		1499.3, 1486.8	**1476.1**, 1471.8	A_1 ScH_2 s. str.
	1454.1	1055.3	1454.1	1066.4	B_1 ScH_2 as. str.
	668.2, 666.5	524.6			B_2 HCCH IP as. bend
	577.7		567.7	505.5	A_1 ScH_2 scis.
i	1406.9, 1401.4, 1381.5	1015.8, 1008.3, 995.1	1406.9, 1401.4, 1381.4	covered, 1013.3	A′ Sc−H str.
	1357.4		1323.2		A′ CH_2 scis.
	covered		covered		A″ HCCH OOP bend
	862.0	644.5	857.0		A″ CH_2 wag
	524.8				A′ C−Sc str.
h	1507		1485		higher-order product

[a] All frequencies are in cm^{-1}. Stronger absorptions in a set are bold. Description gives the major coordinate. The **d**, **i**, and h stand for the dihydrido cyclic, insertion, and high-order products, respectively.

TABLE 2: Observed and Calculated Frequencies of the Fundamental Bands of $HSc-CHCH_2$ in Its Ground $^2A''$ State[a]

	$HSc-CHCH_2$				$DSc-CDCD_2$				$HSc-^{13}CH^{13}CH_2$			
description	obs.[b]	BPW91[c]	B3LYP[d]	int.[d]	obs.[b]	BPW91[c]	B3LYP[d]	int.[d]	obs.[b]	BPW91[c]	B3LYP[d]	int.[d]
A′ C−H str.		3085.5	3143.8	9		2287.6	2328.6	1		3075.6	3133.4	10
A′ C−H str.		3035.3	3102.2	17		2236.8	2284.6	6		3026.0	3093.0	18
A′ C−H str.		2795.8	2825.0	93		2046.9	2064.6	53		2788.8	2818.1	92
A′ C═C str.		1572.6	1617.1	1		1462.4	1444.0	10		1542.6	1599.3	3
A′ Sc−H str.	1381.5	1482.9	1416.3	478	995.1	1058.0	1010.2	336	1381.4	1478.9	1413.7	593
A′ CH_2 scis.	1357.4	1391.7	1387.4	205		1048.5	1095.0	15	1323.2	1362.7	1350.4	85
A′ HCCH IP as. bend		1171.8	1215.3	8		967.9	997.8	14		1155.2	1198.4	8
A″ HCCH OOP bend	*e*	978.5	1030.8	102		746.7	773.9	32	*e*	975.6	1026.5	103
A′ HCCH IP s. bend		866.4	897.5	35		629.6	648.8	18		864.1	895.7	34
A″ CH_2 wag	862.0	901.8	863.3	101	644.5	701.9	678.7	88	857.0	892.0	854.6	97
A′ C−Sc str.	524.8	554.3	545.2	64		507.1	490.3	41		542.0	533.0	64
A″ CH_2 twist		344.9	367.6	25		258.6	286.0	20		343.1	365.9	25
A′ CScH bend		327.8	315.5	50		260.5	276.3	17		325.9	310.2	54
A′ CCSc bend		222.0	237.8	150		184.3	178.8	91		217.9	235.8	144
A″ ScH OOP bend		40.3	83.5	234		29.6	61.7	116		40.2	83.3	235

[a] Frequencies and intensities are in cm^{-1} and km/mol, respectively. [b] Observed in an argon matrix. [c] Frequencies computed with BPW91/6-311++G(3df,3pd). [d] Frequencies and intensities computed with B3LYP/6-311++G(3df,3pd). SDD core potential and basis set are used for Sc. [e] Covered. $HSc-CHCH_2$ has a planar structure.

metals.[12,14] The energies of the H_2-elimination products relative to the metal dihydrido cyclic complexes correlate with the observed results.[11–14]

In this study, we report matrix IR spectra from reactions of laser-ablated Group 3 metal atoms with ethylene isotopomers. The identified primary products are compared with those of the previous studies for Groups 4−6 metals and actinides (Th and U).[10–14] Evidently, the H_2-elimination efficiency shows a substantial variation among Group 3 metals. DFT computations reproduce the stability of the identified products, their vibrational characteristics, and the reaction path.

Experimental Computational Methods

The experimental apparatus has been described previously.[6,15] Laser-ablated Group 3 metal atoms (Johnson-Matthey), produced by laser ablation of metal targets with a Nd:YAG laser (5 to 20 mJ/pulse), were reacted with C_2H_4, C_2D_4, $^{13}C_2H_4$ (Cambridge Isotope Laboratories, 99%), and CH_2CD_2 (MSD Isotopes) in excess argon during condensation at 10 K using a closed-cycle refrigerator (Air Products Displex). Reagent gas mixtures ranged from 0.5 to 1.0% in argon. After reaction, infrared spectra were recorded at a resolution of 0.5 cm^{-1} using a Nicolet 550 spectrometer with an MCT range B detector. Samples were later irradiated for 20 min periods by a mercury arc street lamp (175 W) with the globe removed and a combination of optical filters and subsequently annealed to allow further reagent diffusion.[15]

In order to support the assignment of new experimental frequencies, and to correlate with our previous investigations,[11–14] similar density functional theory (DFT) calculations were carried out using the Gaussian 03 package,[16] B3LYP density functional,[17] 6-311++G(3df,3pd) basis sets for C, H, and Sc,[18] and the SDD pseudopotential and basis set[19] for Y and La to provide a consistent set of vibrational frequencies for the reaction products. Geometries were fully relaxed during optimization, and the optimized geometry was confirmed by vibrational analysis. BPW91[20] calculations were also done to complement the B3LYP results. The vibrational frequencies were calculated analytically, and the zero-point energy was included in the calculation of binding energies. Previous investigations have shown that DFT calculated harmonic frequencies are usually slightly higher than the observed anharmonic frequencies,[6,11–15,21] and they provide useful predictions for infrared spectra of new molecules.

Results and Discussion

Reactions of laser-ablated Group 3 metal atoms with ethylene isotopomers were carried out, and the matrix infrared spectra of new products will be compared with frequencies calculated by density functional theory.

Sc + C_2H_4. Figure 1 shows the C_2H_4, $^{13}C_2H_4$, C_2D_4, and CH_2CD_2 spectra in the Sc−H stretching frequency region. The product absorptions are relatively weak in comparison with the previous early transition metal cases (Groups 4−6),[11–13] consistent with the low reactivity of Group 3 metals in previous studies.[4] Two sets of primary product absorptions marked **i** and **d** are observed on the basis of the intensity variations upon photolysis and annealing. (**i** and **d** denote insertion and dihydrido

cyclic products.) The **i** absorptions triple upon visible ($\lambda > 420$ nm) irradiation, increase another 100% upon UV ($240 < \lambda < 380$ nm) irradiation (a quadruple in total), and gradually decrease in the process of annealing. The **d** absorptions, on the other hand, are almost invisible in the original spectra but emerge upon visible irradiation and triple upon UV photolysis from the intensities after visible irradiation. The observed frequencies of the product (**i** and **d**) absorptions are listed in Table 1 and compared with the DFT computed frequencies in Tables 2 and 3.

The **i** absorptions in the Sc−H stretching region at 1406.9, 1401.4, and 1383.5 cm^{-1} probably split due to different matrix cages, show essentially no ^{13}C shifts, and have their D counterparts at 1015.8, 1008.3, and 995.1 cm^{-1} (H/D ratios of 1.385, 1.390, and 1.390), as illustrated in Figures 1 and 2 and in Table 1. They are also compared with the hydrogen stretching frequencies of 1530.4 cm^{-1} for ScH, 1487.7 cm^{-1} for ScH_3, and 1414.1 and 1360.9 cm^{-1} for $(H_2)ScH_2$ and the deuterium counterparts of 1103.4 cm^{-1} for ScD, 1079.1 cm^{-1} for ScD_3, and 980 cm^{-1} for $(D_2)ScD_2$.[22] The scandium hydride absorptions are not observed in this study. The Sc−H stretching **i** absorptions, whose frequencies are comparable to those of $(H_2)ScH_2$, suggest that the reaction product responsible for the **i** absorptions contains a ScH moiety generated via C−H insertion by Sc. It is most probably the insertion complex ($HSc-C_2H_3$) on the basis of the previous studies.[6,10–14] The BPW91 and B3LYP computed Sc−H stretching frequencies of 1482.9 and 1416.3 cm^{-1} for $HSc-C_2H_3$ are also in line with this conclusion.

The other observed **i** absorptions all support formation of the insertion complex as well. The weak **i** absorption at 1357.4 cm^{-1} has its ^{13}C counterpart at 1323.2 cm^{-1} (12/13 ratio of 1.026) and is assigned to the A′ CH_2 scissoring mode without observation of the D counterpart, which is heavily coupled with the C═C stretching mode. The **i** absorption at 862.0 has its D and ^{13}C counterparts at 644.5 and 857.0 cm^{-1} (H/D and 12/13 ratios of 1.337 and 1.006) and is assigned to the CH_2 wagging mode on the basis of the frequency and large D shift. Another **i** absorption in the low-frequency region at 524.8 is assigned to the C−Sc stretching mode without observation of the D and ^{13}C counterparts. The observed **i** absorptions, which correspond to the strong vibrational bands predicted for $HSc-C_2H_3$ in the ground $^2A''$ state, substantiate formation of the insertion product.

The **d** absorptions in the Sc−H stretching region at 1499.8, 1487.3, and 1454.1 cm^{-1}, among which the two high-frequency absorptions are most probably the antisymmetric ScH_2 stretching absorptions split by the matrix, show negligible ^{13}C shifts. The D counterpart of the symmetric ScH_2 stretching absorption at 1454.1 cm^{-1} is observed at 1055.3 cm^{-1} (H/D ratio of 1.378), but those for the antisymmetric absorptions are unfortunately covered by a precursor band. These **d** absorptions in the Sc−H stretching region indicate that another major product resulting from rearrangement following the C−H insertion is produced, and the **d** absorptions, in view of the previous studies[10–14] and computation results, most probably arise from the dihydrido cyclic complex, $H_2Sc-C_2H_2$. Table 3 shows that the BPW91 ScH_2 stretching frequencies of 1514.9 and 1470.7 cm^{-1} and the B3LYP frequencies of 1551.7 and 1501.1 cm^{-1} for $H_2Sc-C_2H_2$ are in accord with the observed frequencies.

Moreover, the **d** absorptions at 668.2 and 666.5 cm^{-1} have the D counterpart at 524.6 cm^{-1} (H/D ratios of 1.275 and 1.270), and they are assigned to the B_2 HCCH in-plane bending mode on the basis of the frequency and relatively large D shifts. Another **d** absorption at 577.7 cm^{-1} has its ^{13}C counterpart at 567.7 cm^{-1} (12/13 ratio of 1.018), but the D counterpart is

TABLE 3: Observed and Calculated Frequencies of the Fundamental Bands of $H_2Sc-C_2H_2$ in Its Ground $^2B_2$ State[a]

	$H_2Sc-C_2H_2$				$D_2Sc-C_2D_2$			$H_2Sc-{}^{13}C_2H_2$			HDSc−CHCD		
description	obs.[b]	BPW91[c]	B3LYP[d]	int.[d]	obs.[b]	BPW91[c]	B3LYP[d]	int.[d]	obs.[b]	BPW91[c]	B3LYP[d]	int.[d]	obs.[b]	BPW91[c]	B3LYP[d]	int.[d]
A_1 C−H str.		3190.6	3251.2	4		2464.0	2511.2	21		3173.5	3233.7	3		3163.9	3223.9	5
B_2 C−H str.		3133.4	3192.8	6		2297.2	2340.8	3		3124.5	3183.7	6		2385.0	2430.5	14
A_1 C═C str.		1740.6	1776.9	34		1607.0	1639.2	39		1680.5	1716.1	23		1667.7	1701.9	34
A_1 ScH_2 s. str.	1499.8.	1514.9	1551.7	506	*e*	1078.4	1105.1	262	1499.3	1514.6	1551.0	513	1066.4	1069.0	1093.5	358
B_1 ScH_2 as. str.	1454.1	1470.7	1501.1	785	1055.3	1058.7	1080.8	413	1454.1	1470.7	1501.1	785	1476.1	1492.8	1526.2	630
A_1 HCCH IP s. bend		732.0	741.4	32		557.6	548.5	2		730.0	739.5	34		690.1	709.9	83
A_2 HCCH OOP as. bend		677.6	715.2	0		543.8	588.8	0		668.4	705.5	0		648.7	683.8	19
B_2 HCCH IP as. bend	668.2	638.1	677.5	174	524.6	511.3	543.1	100		632.1	671.1	172		532.8	545.6	68
B_1 HCCH OOP s. bend		585.6	613.8	91		440.8	462.0	49		582.7	610.8	90		481.9	505.2	50
A_1 ScH_2 scis.	577.7	589.9	592.6	176		459.7	466.7	101	567.7	588.9	591.3	173	505.5	520.5	535.5	145
A_1 ScC_2 s. str.		393.6	403.5	0		344.6	351.0	9		385.3	395.0	0		381.2	390.9	1
B_2 ScC_2 as. str.		347.9	361.4	31		319.8	331.5	26		337.4	350.8	33		331.6	343.9	33
B_1 ScH_2 rock		284.2	294.1	23		208.6	215.8	9		283.9	293.8	23		233.3	241.1	14
B_2 ScH_2 wag		183.8	203.6	433		134.2	149.0	226		183.6	203.2	430		174.9	191.8	259
A_2 ScH_2 twist		169.8	183.1	0		126.7	136.8	0		168.8	181.9	0		132.0	144.0	67

[a] Frequencies and intensities are in cm^{-1} and km/mol, respectively. [b] Observed in an argon matrix. [c] Frequencies computed with BPW91/6-311++G(3df,3pd). [d] Frequencies and intensities computed with B3LYP/6-311++G(3df, 3pd). SDD core potential and basis set are used for Sc. [e] $H_2Sc-C_2H_2$ has a C_{2v} structure.

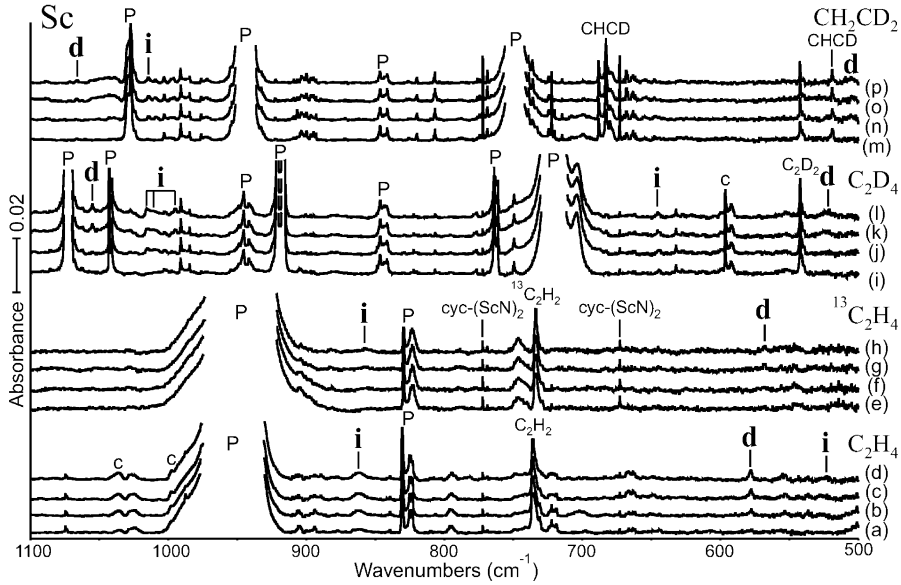

Figure 2. IR spectra in the region of 1100−500 cm^{-1} for laser-ablated Sc atoms codeposited with ethylene isotopomers in excess argon at 10 K and their variation. (a) Sc + 0.5% C_2H_4 in Ar codeposited for 1 h. (b) As (a) after photolysis with $\lambda > 420$ nm. (c) As (b) after photolysis with $240 < \lambda < 380$ nm. (d) As (c) after annealing to 24 K. (e) Sc + 0.5% $^{13}C_2H_4$ in Ar codeposited for 1 h. (f) as (e) after photolysis with $\lambda > 420$ nm. (g) as (f) after photolysis with $240 < \lambda < 380$ nm. (h) as (g) after annealing to 24 K. (i) Sc + 0.5% C_2D_4 in Ar codeposited for 1 h. (j) as (i) after photolysis with $\lambda > 420$ nm. (k) as (j) after photolysis with $240 < \lambda < 380$ nm. (l) as (k) after annealing to 24 K. (m) Sc + 0.5% CH_2CD_2 in Ar codeposited for 1 h. (n) as (m) after photolysis with $\lambda > 420$ nm. (o) as (n) after photolysis with $240 < \lambda < 380$ nm. (p) as (o) after annealing to 24 K. The **i** and **d** denote the product absorption groups, c identifies product absorptions common to the precursor in other metal experiments, P designates unreacted precursor absorptions, cyc-$(ScN)_2$[23] and acetylene isotopomer absorptions are indicated, and w identifies water residue absorptions.

expected in a too low frequency region to observe. It is assigned to the ScH_2 scissoring mode. The observed **d** absorptions all support formation of the Sc dihydrido cyclic complex ($H_2Sc-C_2H_2$), which is originally proposed in reaction dynamics studies as the reaction intermediate prior to H_2-elimination.[1–5] The present results also show that not only the Groups 4−6 early transition metals but the Group 3 metal also undergoes C−H bond insertion of ethylene following rearrangement to the dihydrido cyclic product, from which the H_2 molecule eventually departs.[10–13]

However, absence of the ScH_x absorptions is indicative of the slow H_2-releasing step. Figure 3 shows the energies of the plausible products relative to the reactants ($Sc(^2D) + C_2H_4$), where the insertion complex is the second most stable next to the metallacyclopropane in the doublet potential surface. The dihydrido cyclic complex is 7.9 kcal/mol higher than the insertion complex, and the H_2-elimination products are 1.1 and 6.2 kcal/mol higher than the reactants and the dihydrido cyclic reaction intermediate, respectively. The almost indiscernible **d** absorptions in the original spectra after deposition and the dramatic increase in the following process of photolysis indicate that the original production yield for $H_2Sc-C_2H_2$ during codeposition of the metal atoms and ethylene is minor, but it is mostly produced on the subsequent photolysis via the insertion complex.[5]

The metallacyclopropane ($Sc-C_2H_4$) is energetically most stable among the plausible products, as shown in Figure 3, but unfortunately, its absorptions are predicted to be all very weak, as shown in Table S1 (Supporting Information). Moreover, the strongest C−C stretching band (41 km/mol) expected at ∼960 cm^{-1} would be covered by a strong precursor band. The elusive metallacyclopropane absorptions[13] are not observed in this study from reactions of Group 3 metals, although it is believed to be one of the major products. The trihydrido ethynyl complex[11,14] is energetically too high in comparison with other plausible

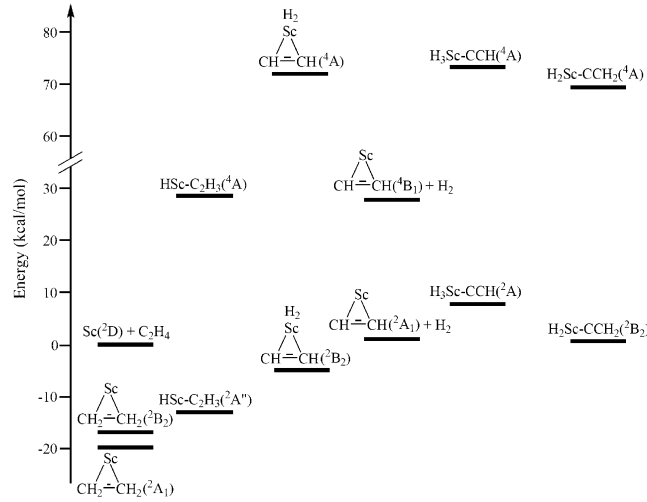

Figure 3. The energies of the plausible products relative to the reactants ($Sc(^2D)$ + ethylene). Notice that the metallacyclopropane ($Sc-C_2H_4$), insertion ($HSc-C_2H_3$), and dihydrido cyclic ($H_2Sc-C_2H_2$) complexes in the doublet ground states are the most stable ones. The insertion and dihydrido cyclic products are identified from the matrix IR spectra (see text). The H_2-elimination product ($Sc-C_2H_2(^2A_1) + H_2$) is 1 kcal/mol higher than the reactants, and no ScH_x absorptions are observed in this study.

products, and two of the ScH_3 stretching absorptions would appear in the low-frequency region below 800 cm^{-1}, which are not observed. The vinylidene complex ($H_2Sc-CCH_2$) would show another ScH_2 stretching absorption pair at about 20 cm^{-1} higher than those of the dihydrido cyclic product and a strong ScH_2 scissoring absorption at about 600 cm^{-1}, which are not observed as well. The product absorptions marked h at 1507 and 1485 cm^{-1} in the C_2H_4 and $^{13}C_2H_4$ continuously increase upon photolysis and annealing, and they are assigned to absorptions of a higher-order product.

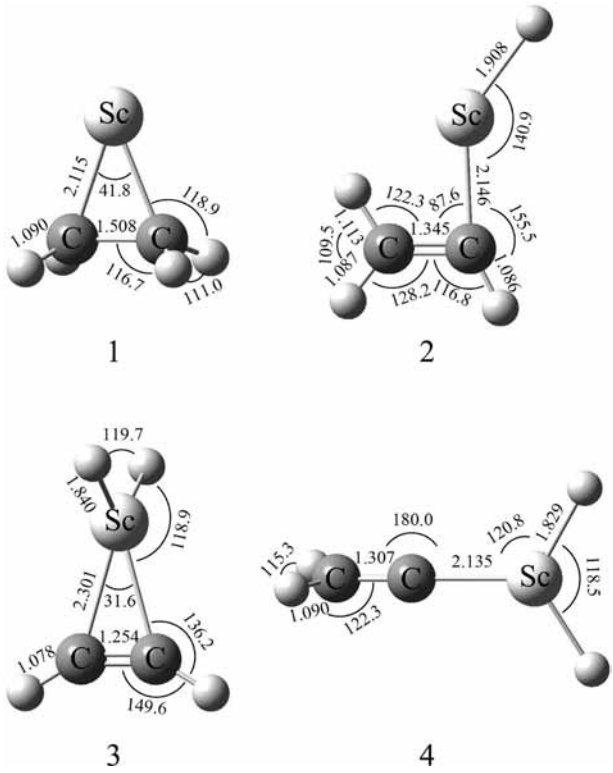

Figure 4. The B3LYP structures of the most plausible products from reaction of Sc atoms with ethylene. The metallacyclopropane ($Sc-C_2H_4$) complex (1) has a C_{2v} structure, the insertion complex ($HSc-C_2H_3$) (2) a planar C_s structure, and the dihydrido cyclic ($H_2Sc-C_2H_2$) (3) and vinylidene ($H_2Sc-CCH_2$) (4) complexes have C_{2v} structures. The illustrated structures are for the doublet ground states.

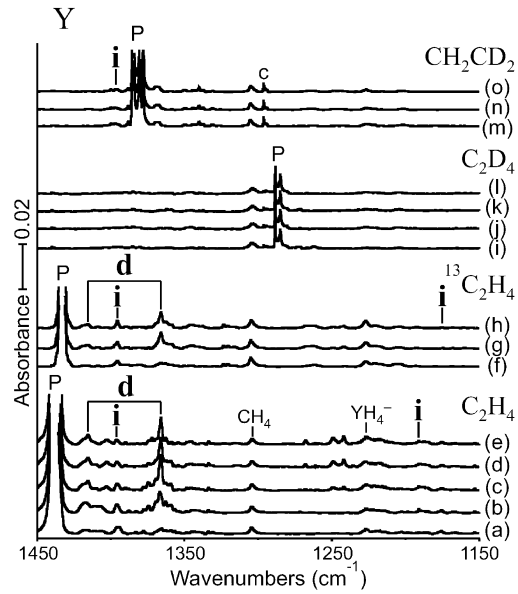

Figure 5. IR spectra in the region of 1450−1150 cm^{-1} for laser-ablated Y atoms codeposited with ethylene isotopomers in excess argon at 10 K and their variation. (a) Y + 0.5% C_2H_4 in Ar codeposited for 1 h. (b) As (a) after photolysis with $\lambda > 420$ nm. (c) As (b) after photolysis with $240 < \lambda < 380$ nm. (d) As (c) after photolysis with $\lambda > 220$ nm. (e) as (d) after annealing to 24 K. (f) Y + 0.5% $^{13}C_2H_4$ in Ar codeposited for 1 h. (g) as (f) after photolysis with $\lambda > 220$ nm. (h) as (g) after annealing to 24 K. (i) Y + 0.5% C_2D_4 in Ar codeposited for 1 h. (j) as (i) after photolysis with $\lambda > 420$ nm. (k) as (j) after photolysis with $240 < \lambda < 380$ nm. (l) as (k) after annealing to 24 K. (m) Y + 0.5% CH_2CD_2 in Ar codeposited for 1 h. (n) as (m) after photolysis with $\lambda > 220$ nm. (o) as (n) after annealing to 24 K. The **i** and **d** denote the product absorption groups, c identifies product absorptions common to the precursor in other metal experiments, and P designates unreacted precursor absorptions. The YH_4^- absorption is also indicated.

Therefore, it is believed that the metallacyclopropane and insertion complexes are the primary reaction products captured in the matrix after deposition, and dihydrido cyclic complexes are mostly produced in the following process of photolysis. No other considerable reaction products are identified from the matrix IR spectra. Evidently, the reaction of Sc with ethylene occurs in the doublet potential surface, as previous reaction dynamics studies also presume. The insertion and dihydrido cyclic complexes in the quartet states are simply too high in energy (28.5 and 72.0 kcal/mol higher than the reactants), not to mention the probability of reaching the quartet surface from the reactants ($Sc(^2D) + C_2H_4$).

Figure 4 illustrates the structures of the plausible products from reaction of Sc with ethylene. The C−C and C−Sc bonds of the metallacyclopropane are the longest and shortest among those of the plausible products, indicating that the Sc−C bonds are strong single bonds, and as a result, the C−C double bond weakens. Interestingly enough, the C−Sc bonds of the dihydrido cyclic complex ($H_2Sc-C_2H_2$) are the longest, in contrast to the previous cases of Groups 4−6 metals and actinides, where the metal−carbon bonds are the shortest among those of the plausible products. Sc($[Ar]3d^14s^2$) is most electron-deficient among the first-row transition metals, and therefore, in the doublet ground state, the four bonds of Sc with two hydrogen and two carbon atoms are expected to be weak. Moreover, the back-donation from the metal center to the cyclic π-system in the dihydrido cyclic complex, which is estimated to be substantial in the previously studied early transition-metal and actinide systems, is also believed to be insignificant on the basis of the short C−C bond.

Y + C_2H_4. Shown in Figure 5 are the product matrix IR spectra in the Y−H stretching absorption region from reactions of laser-ablated Y atoms with ethylene isotopomers. Similar to the Sc case described above, two sets of product absorptions marked **i** and **d** (**i** and **d** for insertion and dihydrido cyclic complexes) are observed on the basis of the intensity variations upon photolysis and annealing. The **i** absorptions slightly increase upon visible irradiation but decrease upon the following UV and full arc ($\lambda > 220$ nm) photolysis to a half of the original intensity. On the other hand, the **d** absorptions are very weak in the original spectra after deposition but are quadruple upon visible photolysis and increase another 300% upon UV irradiation (700% increase in total). They latter slightly decrease upon full arc irradiation and gradually decrease in annealing. Unlike the Sc case, the YH_4^- absorption is observed at 1227.3 cm^{-1}; however, the D counterpart is not observed. The weak YH_2^+ absorption is also observed at 1542.5 cm^{-1}, but no other YH_x absorptions are noticed in the spectra.[22] The product absorption frequencies are listed in Table 4, and the DFT frequencies for the insertion, dihydrido cyclic, and metallacyclopropane are listed in Tables 5, 6 and S2 (Supporting Information).

The **i** absorption at 1396.2 cm^{-1} shows no ^{13}C shift and has its D counterpart at 1006.6 cm^{-1} (H/D ratio of 1.387), as shown in Figures 5 and 6. They are compared with the hydrogen stretching frequencies of 1470.4 cm^{-1} for YH, 1459.8 and 1397.8 cm^{-1} for YH_2, and 1385.1 cm^{-1} for YH_3 and the D counterparts of 1053.1 cm^{-1} for YD, 1042.0 and 1003.2 cm^{-1} for YD_2, and 995.3 cm^{-1} for YD_3.[22] The observed Y−H stretching frequency close to those of YH_2 suggests that the primary product responsible for the **i** absorption has a HY− moiety, and most probably, it is again the insertion product, $HY-C_2H_3$.[10−14] The other observed **i** absorptions also support

TABLE 4: Frequencies of Product Absorptions Observed from Reactions of Y with Ethylene in Excess Argon[a]

	C_2H_4	C_2D_4	$^{13}C_2H_4$	CH_2CD_2	description
d	1689.2				A_1 C═C str.
	1415.6	1014.5	1415.7		A_1 YH_2 s. str.
	1374.6, **1366.2**	984.5, **982.4**	1366.2	997.3	B_1 YH_2 as. str.
	659.8	506.8	656.3		B_2 HCCH IP as. bend
	568.6		533.8		B_1 HCCH OOP s. bend
	522.5		521.0		A_1 YH_2 scis.
i	1396.2	1006.6	1395.9	1396.1, 1006.0	A′ Y−H str.
	1190.9		1175.1	1102.1	A′ HCCH IP as. bend
	893.9				A′ HCCH IP s. bend
	506.8		483.7		A′ C−Y str.
YH_x	1542.5		1542.5		YH_2^+
	1227.3		1542.5	1542.5	YH_4^-

[a] All frequencies are in cm^{-1}. Stronger absorptions in a set are bold. Description gives the major coordinate. The **d** and **i** stand for the dihydrido cyclic and insertion products, respectively. YH_x designates yttrium hydrides.

TABLE 5: Observed and Calculated Frequencies of the Fundamental Bands of $HY-CHCH_2$ in Its Ground $^2A'$ State[a]

	$HY-CHCH_2$				$DY-CDCD_2$				$HY-^{13}CH^{13}CH_2$			
description	obs.[b]	BPW91[c]	B3LYP[d]	int.[d]	obs.[b]	BPW91[c]	B3LYP[d]	int.[d]	obs.[b]	BPW91[c]	B3LYP[d]	int.[d]
A′ C−H str.		3076.7	3134.1	17		2279.2	2322.2	6		3066.6	3123.7	17
A′ C−H str.		3029.6	3094.5	26		2232.8	2280.4	12		3020.4	3085.2	26
A′ C−H str.		2823.7	2894.3	49		2067.1	2118.6	21		2816.6	2887.0	50
A′ C═C str.		1566.1	1612.7	4		1462.7	1499.1	1		1535.1	1583.2	6
A′ Y−H str.	1396.2	1427.8	1448.7	526	1006.6	1015.3	1030.2	272	1395.8	1427.8	1448.7	525
A′ CH_2 scis.		1390.0	1427.8	11		1046.6	1081.8	13		1362.1	1396.9	9
A′ HCCH IP as. bend	1190.9	1186.2	1233.2	18		972.5	1008.3	3	1175.1	1170.0	1216.6	19
A″ HCCH OOP bend		1011.6	1048.7	1		761.8	792.3	0		1008.2	1046.0	1
A″ CH_2 wag		916.2	952.0	12		719.9	746.2	7		906.1	941.6	12
A′ HCCH IP s. bend	893.9	884.8	922.0	21		643.0	670.1	11		882.3	919.4	20
A′ C−Y str.	506.8	501.6	504.8	75		456.2	459.1	60	483.7	488.9	492.1	74
A″ CH_2 twist		347.9	358.1	41		260.5	267.9	24		346.2	356.3	40
A′ CYH bend		307.6	313.3	57		232.5	236.2	23		306.4	312.0	57
A′ CCY bend		199.0	192.9	37		171.7	167.0	32		194.5	188.5	35
A″ YH OOP bend		94.6	121.6	51		67.0	87.1	23		94.7	121.6	51

[a] Frequencies and intensities are in cm^{-1} and km/mol, respectively. [b] Observed in an argon matrix. [c] Frequencies computed with BPW91/6-311++G(3df,3pd). [d] Frequencies and intensities computed with B3LYP/6-311++G(3df,3pd). SDD core potential and basis set are used for Y. $HY-CHCH_2$ has a planar structure.

formation of $HY-C_2H_3$ via C−H insertion by Y. The weak **i** absorption at 1190.9 cm^{-1} has its ^{13}C counterpart at 1175.1 cm^{-1} (12/13 ratio of 1.013), but the weaker D counterpart is probably covered by a precursor absorption at around 945 cm^{-1}. It is assigned to the HCCH antisymmetric in-plane bending mode. Another weak **i** absorption at 893.9 cm^{-1} is assigned to the HCCH symmetric in-plane bending mode on the basis of the DFT frequencies without observation of the D and ^{13}C counterparts. The relatively strong **i** absorption at 506.8 cm^{-1} has its ^{13}C counterpart at 483.7 cm^{-1}, but its D counterpart is located too low to observe. It is assigned to the C−Y stretching mode.

The strong **d** absorptions at 1415.6 and 1366.2 cm^{-1} show no ^{13}C shifts and have D counterparts at 1014.5 and 982.4 cm^{-1} (H/D ratios of 1.395 and 1.391). The observed Y−H stretching absorptions with an intensity ratio of about 1:2 most probably originate from the symmetric and antisymmetric YH_2 stretching modes of the dihydrido cyclic complex, $H_2Y-C_2H_2$, in view of the previous studies.[10–14] The **d** absorption at 659.8 cm^{-1} has its D and ^{13}C counterparts at 506.8 and 656.3 cm^{-1} (H/D and 12/13 ratios of 1.302 and 1.005) and is assigned to the B_2 HCCH in-plane antisymmetric bending mode on the basis of the large D and small ^{13}C shifts. The **d** absorptions at 568.6 and 522.5 cm^{-1} have their ^{13}C counterparts at 533.8 and 521.0 cm^{-1} (12/13 ratios of 1.065 and 1.003), but their D counterparts are located too low in frequency to observe. They are designated to the B_1 HCCH in-plane antisymmetric bending and A_1 YH_2 scissoring modes, respectively. The weak absorption at 1689.2 cm^{-1} (not shown) is assigned to the A_1 C═C stretching mode. The observed six absorptions substantiate generation of the dihydrido cyclic complex, $H_2Y-C_2H_2$, mostly in the process of photolysis, parallel to the Sc case.

The energies of the plausible products relative to the reactants ($Y(^2D) + C_2H_4$) are shown in Figure 7. The metallacyclopropane and insertion complex in the doublet ground states are the most stable among the plausible products from reaction of Y with ethylene, and the dihydrido cyclic complex is 12.6 and 13.9 kcal/mol higher than $Y-C_2H_4$ and $HY-C_2H_3$. Parallel to the Sc case, the relative energies are consistent with the observed intensities of the product absorptions; the **d** absorptions are very weak in the original spectra after deposition and increase later upon photolysis, while the **i** absorptions are relatively strong in the original spectra and decrease later upon UV photolysis. The H_2-elimination products are 6.5 and 2.6 kcal/mol higher than the dihydrido cyclic complex and the reactants, respectively. H_2-elimination by Y is evidently faster than that for the Sc case on the basis of the observed YH_2^+ and YH_4^- absorptions.[22] While the difference is small, the H_2-elimination products by Y is 2.6 kcal/mol lower than the reactants, whereas those by Sc is 1.1 kcal/mol higher.

The reaction is again believed to proceed in the doublet potential surface. The insertion and dihydrido complexes are 42.2 and 68.6 kcal/mol higher in the quartet state than the reactants. The absorption intensities of the Y metallacyclopropane are also predicted to be very weak, as shown in Table S2

TABLE 6: Observed and Calculated Frequencies of the Fundamental Bands of $H_2Y-C_2H_2$ in Its Ground $^2B_2$ State[a]

	$H_2Y-C_2H_2$				$D_2Y-C_2D_2$				$H_2Y-{}^{13}C_2H_2$				HDY−CHCD			
description	obs.[b]	BPW91[c]	B3LYP[d]	int.[d]	obs.[b]	BPW91[c]	B3LYP[d]	int.[d]	obs.[b]	BPW91[c]	B3LYP[d]	int.[d]	obs.[b]	BPW91[c]	B3LYP[d]	int.[d]
A_1 C−H str.		3155.3	3211.1	0		2425.0	2468.2	6		3139.2	3194.8	0		3130.3	3185.7	0
B_2 C−H str.		3102.3	3157.1	1		2273.8	2314.0	0		3093.5	3148.2	1		2353.1	2395.0	4
A_1 C═C str.	1689.2	1719.0	1757.0	24		1599.7	1635.0	21		1658.5	1695.2	21		1654.2	1690.7	22
A_1 YH_2 s. str.	1415.6	1434.7	1458.1	442	1014.5	1017.9	1034.6	228	1415.7	1434.7	1458.1	443	997.3	1006.9	1022.0	347
B_1 YH_2 as. str.	1366.2	1394.2	1413.1	807	982.4	995.3	1008.8	417	1366.2	1394.2	1413.1	807		1414.6	1435.8	604
A_1 HCCH IP s. bend		754.0	773.7	6		559.7	570.2	0		752.0	771.6	7		710.9	735.9	71
A_2 HCCH OOP as.bend		681.8	717.1	0		555.9	588.0	0		672.7	707.5	0		646.4	678.2	17
B_2 HCCH IP as. bend	659.8	656.0	691.8	182	506.8	520.9	548.4	108	656.3	650.2	685.5	179		533.2	557.2	76
B_1 HCCH OOP s. bend	568.6	561.2	576.4	100		418.6	433.6	56	533.8	553.8	573.5	99		499.5	500.2	174
A_1 YH_2 scis.	522.5?	556.5	559.8	219		418.9	419.8	130	521.0	560.6	559.1	217		461.4	477.7	63
A_1 YC_2 s. str.		354.9	360.4	5		323.7	327.2	1		345.4	350.8	6		347.7	353.3	4
B_2 YC_2 as. str.		327.9	337.2	19		301.7	309.8	17		317.4	326.6	19		311.7	320.0	20
B_1 YH_2 rock		273.4	277.4	32		198.8	201.6	14		273.1	277.1	33		223.2	226.2	20
A_2 YH_2 twist		136.1	157.0	0		103.4	119.1	0		135.0	155.7	0		120.4	140.7	53
B_2 YH_2 wag		24.2	90	545		18.6	65.5	281		24.2	90.0	544		20.2	75.0	359

[a] Frequencies and intensities are in cm^{-1} and km/mol, respectively. [b] Observed in an argon matrix. [c] Frequencies computed with BPW91/6-311++G(3df,3pd). [d] Frequencies and intensities computed with B3LYP/6-311++G(3df, 3pd). SDD core potential and basis set are used for Y. $H_2Y-C_2H_2$ has a C_{2v} structure.

(Supporting Information), and the absence of its absorptions indicates that, although it is believed to be a primary product, the complex is not formed in an observable amount. The trihydrido ethynyl complex[11,14] is again energetically too high to be formed, and it would show two of three YH_3 stretching absorptions below 700 cm^{-1}. The vinylidene complex would show another pair of strong YH_2 stretching absorptions at around 1400 cm^{-1} and the strong YH_2 scissoring band at about 550 cm^{-1}, which are not observed in this study.

Figure 8 illustrates the B3LYP structures of the most plausible products, which are similar to those of the Sc products. The C−C bond of the metallacyclopropane is the longest among those of the plausible complexes, whereas the C−Y bond is the shortest, showing that the strong C−Y bonds as a result of strong coordination of the Group 3 metal lead to the weak C−C double bond. Again, the C−Y bonds of the dihydrido cyclic complex are the longest among those of the Y complexes due to electron-deficient Sc. The shortest C−C bond also indicates that back-donation of the Group 3 metal to the π-cyclic system is much weaker than the previously studied early transition metal dihydrido cyclic complexes.

La + C_2H_4. Figure 9 shows the ethylene isotopomer spectra in the La−H stretching frequency regions, where the product absorptions marked **i** are observed, whereas **d** absorptions are not observed in contrast to the Sc and Y cases. The **i** absorptions nearly double upon visible photolysis, slightly increase upon UV irradiation, and slightly decrease upon full arc photolysis. Interestingly enough, along with the **i** absorptions, many lanthanum hydride absorptions are observed. They are the LaH absorption at 1344.1 cm^{-1}, LaH_2 absorptions at 1320.9 and 1283.0 cm^{-1}, LaH_3 absorption at 1263.3 cm^{-1}, $(H_2)LaH_2$ absorptions at 1287.1 and 1235.3 cm^{-1}, $(H_2)_2LaH_2$ absorption at 1221 cm^{-1}, and LaH_4^- absorption at 1114.3 cm^{-1}.[22] The LaD_3 absorption at 904.5 cm^{-1}, $(D_2)LaD_2$ absorption at 884.5 cm^{-1}, and LaD_4^- absorption at 797.8 cm^{-1} are also observed (see Table 7), as shown in Figure 10.[22] These LaH_x absorptions, which also increase in the process of photolysis, demonstrate that H_2-elimination of ethylene by La is much faster during deposition and upon photolysis than that for the Sc and Y cases, where no scandium hydride absorptions are observed in Figures 1 and 2 while only the weak YH_4^- absorption is shown in Figure 5. In addition, the product absorptions in the C_2H_4 and $^{13}C_2H_4$ spectra marked h continuously increase upon photolysis (particularly upon UV photolysis) and annealing, and they are attributed to a higher-order product.

The **i** absorption at 1270.5 cm^{-1} shows negligible ^{13}C shift and has its D counterpart at 908.9 cm^{-1} (H/D ratio of 1.398). The single Sc−H stretching absorption most probably originates from the insertion complex on the basis of the previous studies and with the reasonable agreement with the BPW91 and B3LYP values of 1334.3 and 1358.1 cm^{-1}. The other observed **i** absorptions also support formation of $HLa-C_2H_3$, as shown in Table 8. The **i** absorption at 1198.1 cm^{-1} has its ^{13}C counterpart at 1171.2 cm^{-1}, but its D counterpart is unfortunately covered by a precursor band at 950 cm^{-1}. It is assigned to the A′ HCCH antisymmetric in-plane bending mode. The **i** absorptions at 882.1 and 469 cm^{-1} have their ^{13}C counterparts at 880.8 and 455 cm^{-1}, and they are designated to the A′ HCCH symmetric in-plane bending and C−La stretching modes without observation of the D counterparts. They correspond to the vibrational bands predicted as the strongest for the insertion complex and show good agreement with the DFT frequencies. Consequently, Group 3 metals all readily undergo C−H bond insertion with ethylene.

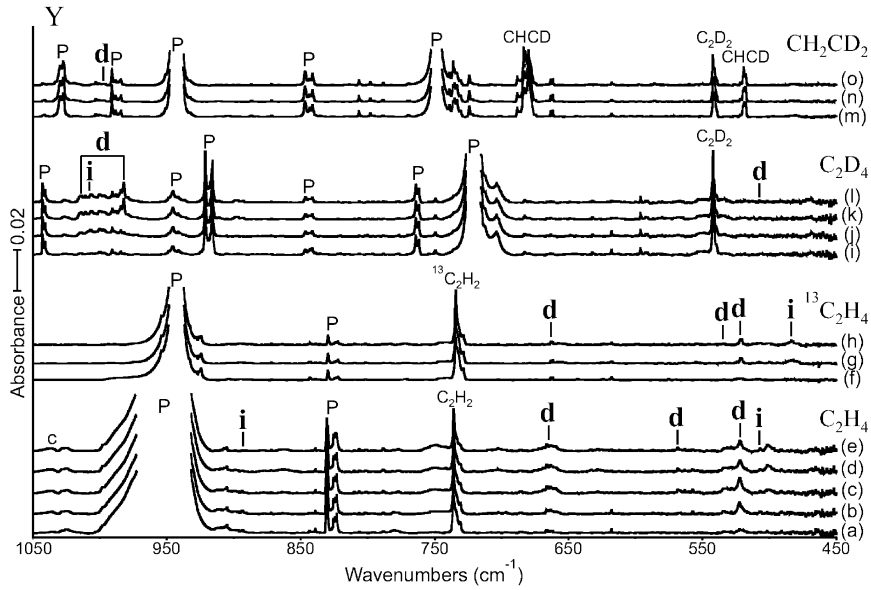

Figure 6. IR spectra in the region of 1050−450 cm^{-1} for laser-ablated Y atoms codeposited with ethylene isotopomers in excess argon at 10 K and their variation. (a) Y + 0.5% C_2H_4 in Ar codeposited for 1 h. (b) As (a) after photolysis with $\lambda > 420$ nm. (c) As (b) after photolysis with $240 < \lambda < 380$ nm. (d) As (c) after photolysis with $\lambda > 220$ nm. (e) as (d) after annealing to 24 K. (f) Y + 0.5% $^{13}C_2H_4$ in Ar codeposited for 1 h. (g) as (f) after photolysis with $\lambda > 220$ nm. (h) as (g) after annealing to 24 K. (i) Y + 0.5% C_2D_4 in Ar codeposited for 1 h. (j) as (i) after photolysis with $\lambda > 420$ nm. (k) as (j) after photolysis with $240 < \lambda < 380$ nm. (l) as (k) after annealing to 24 K. (m) Y + 0.5% CH_2CD_2 in Ar codeposited for 1 h. (n) as (m) after photolysis with $\lambda > 220$ nm. (o) as (n) after annealing to 24 K. The **i** and **d** denote the product absorption groups, c identifies product absorptions common to the precursor in other metal experiments, and P designates unreacted precursor absorptions. Acetylene isotopomer absorptions are also indicated.

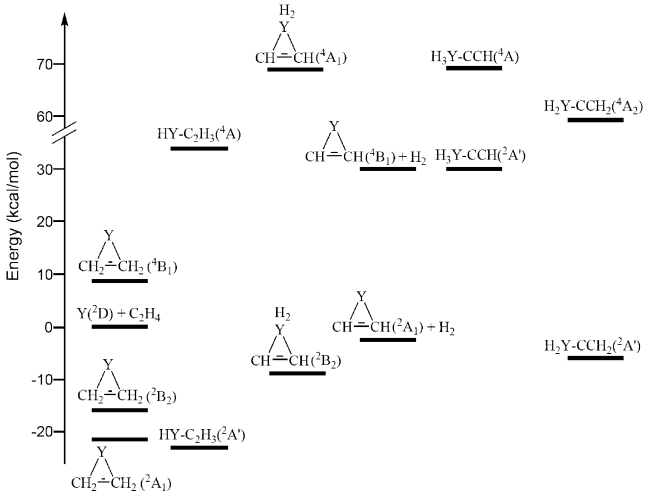

Figure 7. The energies of the plausible products relative to the reactants ($Y(^2D)$ + ethylene). Notice that the metallacyclopropane, insertion, and dihydrido cyclic complexes in the doublet ground states are the most stable ones. The insertion and dihydrido cyclic products are identified from the matrix IR spectra (see text). The H_2-elimination product ($Y-C_2H_2(^2A_1) + H_2$) is 2.6 kcal/mol lower than the reactants, and YH_4^- absorption is observed in this study.

The several observed lanthanum hydride absorptions in the product spectra with ethylene isotopomers suggest that the H_2-elimination of ethylene with La is much faster. Figure 11 illustrates the relative energies of the plausible products and clearly shows that the insertion complex is the most stable along with the metallacyclopropane. On the other hand, the dihydrido cyclic complex is 16.4 kcal/mol higher than the insertion complex, which is compared with the energy differences of 7.9 and 13.9 kcal/mol in the Sc and Y systems, respectively. Parallel to the Sc and Y cases, the trihydrido ethynyl complex[11,14] is energetically very unstable, while no product absorptions are attributable to the trihydrido and vinylidene complexes.

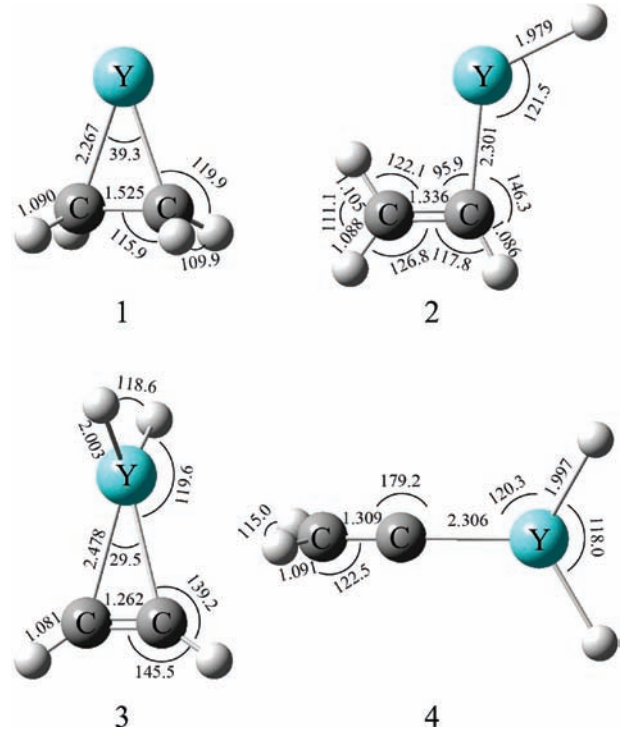

Figure 8. The B3LYP structures of the most plausible products from reaction of Y atoms with ethylene. The metallacyclopropane (1) has a C_{2v} structure, the insertion complex (2) a planar C_s structure, the dihydrido cyclic product (3) a C_{2v} structure, and the vinylidene complex (4) an allene-type C_s structure. The illustrated structures are for the doublet ground states.

Apparently, the La dihydrido cyclic intermediate generated during deposition and subsequent photolysis promptly either converts to the insertion complex or proceeds to the H_2-elimination as this possible product (computed frequencies in Table 9) is not observed here. Moreover, the H_2-elimination

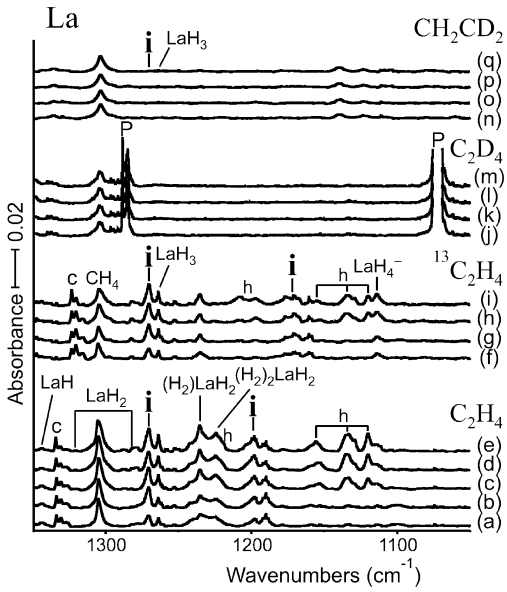

Figure 9. IR spectra in the region of 1350−1050 cm^{-1} for laser-ablated La atoms codeposited with ethylene isotopomers in excess argon at 10 K and their variation. (a) La + 0.5% C_2H_4 in Ar codeposited for 1 h. (b) As (a) after photolysis with $\lambda > 420$ nm. (c) As (b) after photolysis with $240 < \lambda < 380$ nm. (d) As (c) after photolysis with $\lambda > 220$ nm. (e) as (d) after annealing to 24 K. (f) La + 0.5% $^{13}C_2H_4$ in Ar codeposited for 1 h. (g) as (f) after photolysis with $\lambda > 420$ nm. (h) as (g) after photolysis with $240 < \lambda < 380$ nm. (i) as (h) after annealing to 24 K. (j) La + 0.5% C_2D_4 in Ar codeposited for 1 h. (k) as (j) after photolysis with $\lambda > 420$ nm. (l) as (k) after photolysis with $240 < \lambda < 380$ nm. (m) as (l) after annealing to 24 K. (n) La + 0.5% CH_2CD_2 in Ar codeposited for 1 h. (o) as (n) after photolysis with $\lambda > 420$ nm. (p) as (o) after photolysis with $240 < \lambda < 380$ nm. (q) as (p) after annealing to 24 K. The **i** and h denote the product absorption groups, c identifies product absorptions common to the precursor in other metal experiments, and P designates unreacted precursor absorptions. LaH_x absorptions are also indicated.[22]

products are 1.2 and 16.6 kcal/mol lower than $H_2La-C_2H_2$ and the reactants ($La(^2D) + C_2H_4$), respectively. The increasing H_2-elimination rate with going down the group column correlates with the energy of the H_2-elimination products relative to that of the dihydrido cyclic complex in our experiment. A similar tendency is also observed from the previous studies;[11–14] strong metal hydride absorptions are observed only from the systems (e.g., Group 5 metals + ethylene) where the energies of the H_2-elimination products are relatively low regarding those of the dihydrido cyclic intermediate.

The most plausible La reaction products from reaction with ethylene are illustrated in Figure 12. The C−La bonds of the metallacyclopropane and dihydrido cyclic complex are the shortest and longest, respectively, parallel to the Sc and Y cases, while the reverse is true in the previously studied Groups 4−6 transition-metal and actinide systems.[11–14] The difference in the carbon−metal bonds of the two complexes increases with going down the column, 0.185, 0.211, and 0.280 Å for the Sc, Y, and La systems, respectively. Clearly, the electron-deficient Group 3 metals cannot afford four strong bonds with two H and two C atoms for the dihydrido cyclic complex, and the back-donation to the triangular π-cyclic system is also insignificant on the basis of the exceptionally short C−C bond.

Conclusions

Reactions of laser-ablated Group 3 metal atoms with ethylene have been carried out, and the primary products are identified in the matrix IR spectra on the basis of their vibrational characteristics. The insertion ($HM-C_2H_3$) and dihydrido cyclic ($H_2M-C_2H_2$) complexes are identified in the product spectra from reactions of Sc and Y, where the originally weak $H_2M-C_2H_2$ absorptions increase dramatically in the process of photolysis. On the other hand, in the La spectra, only the absorptions from the insertion product are observed along with many lanthanum hydride absorptions. These and other evidence

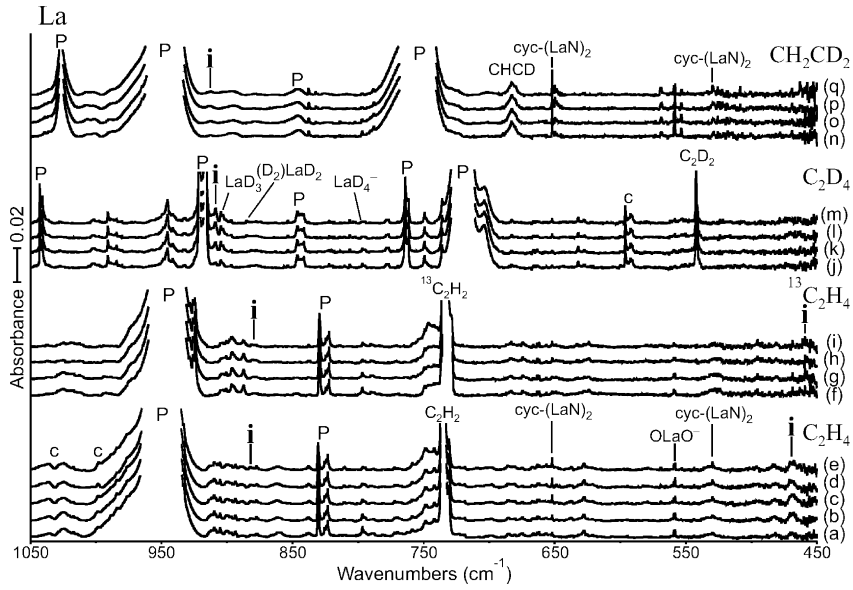

Figure 10. IR spectra in the region of 1050−450 cm^{-1} for laser-ablated La atoms codeposited with ethylene isotopomers in excess argon at 10 K and their variation. (a) La + 0.5% C_2H_4 in Ar codeposited for 1 h. (b) As (a) after photolysis with $\lambda > 420$ nm. (c) As (b) after photolysis with $240 < \lambda < 380$ nm. (d) As (c) after photolysis with $\lambda > 220$ nm. (e) as (d) after annealing to 24 K. (f) La + 0.5% $^{13}C_2H_4$ in Ar codeposited for 1 h. (g) as (f) after photolysis with $\lambda > 420$ nm. (h) as (g) after photolysis with $240 < \lambda < 380$ nm. (i) as (h) after annealing to 24 K. (j) La + 0.5% C_2D_4 in Ar codeposited for 1 h. (k) as (j) after photolysis with $\lambda > 420$ nm. (l) as (k) after photolysis with $240 < \lambda < 380$ nm. (m) as (l) after annealing to 24 K. (n) La + 0.5% CH_2CD_2 in Ar codeposited for 1 h. (o) as (n) after photolysis with $\lambda > 420$ nm. (p) as (o) after photolysis with $240 < \lambda < 380$ nm. (q) as (p) after annealing to 24 K. The **i** denotes the product absorption group, c identifies product absorptions common to the precursor in other metal experiments, and P designates unreacted precursor absorptions. Acetylene isotopomer, LaH_x,[24] and $OLaO^-$[25] absorptions are also indicated.

TABLE 7: Frequencies of Product Absorptions Observed from Reactions of La with Ethylene in Excess Argon[a]

	C_2H_4	C_2D_4	$^{13}C_2H_4$	CH_2CD_2	description
i	1270.5	908.9	1270.5	1270.6	A′ La−H str.
	1198.1		1171.2		A′ HCCH IP as. bend
	882.1		880.8	912.7	A′ HCCH IP s. bend
	469		455		A′ C−La str.
h	1223		1208, 1197		high-order product
	1154, **1134**, 1121		1155, 1134, 1121		high-order product
LaH_x	1344.1		1344.1		LaH
	1320.9, 1283.0		1283.0		LaH_2
	1263.3	904.5	1263.3	1263.3	LaH_3
	1287.1, 1235.3	884.5	1287.1, **1235.3**		$(H_2)LaH_2$
	1221		1221		$(H_2)_2LaH_2$
	1114.3	797.8	1114.3		LaH_4^-

[a] All frequencies are in cm^{-1}. Stronger absorptions in a set are bold. Description gives the major coordinate. The **i** and h stand for the insertion and high-order products, respectively. LaH_x designates lanthanum hydrides.

TABLE 8: Observed and Calculated Frequencies of the Fundamental Bands of $HLa-CHCH_2$ in Its Ground $^2A'$ State[a]

	$HLa-CHCH_2$				$DLa-CDCD_2$				$HLa-^{13}CH^{13}CH_2$			
description	obs.[b]	BPW91[c]	B3LYP[d]	int.[d]	obs.[b]	BPW91[c]	B3LYP[d]	int.[d]	obs.[b]	BPW91[c]	B3LYP[d]	int.[d]
A′ C−H str.		3057.2	3117.0	27		2268.2	2312.8	10		3046.8	3106.3	28
A′ C−H str.		3027.8	3090.8	21		2228.9	2275.2	11		3018.8	3081.7	21
A′ C−H str.		2859.0	2931.3	45		2090.7	2143.7	20		2852.0	2924.1	46
A′ C═C str.		1565.7	1610.8	2		1467.4	1503.5	1		1532.5	1579.0	3
A′ CH_2 scis.		1386.1	1424.7	17		1040.4	1075.7	12		1360.4	1396.0	18
A′ La−H str.	1270.5	1334.3	1358.1	743	908.9	946.6	963.7	369	1270.5	1334.3	1358.0	739
A′ HCCH IP as. bend	1198.1	1178.5	1228.0	17		965.2	1002.0	13	1171.2	1162.4	1211.6	18
A″ HCCH OOP bend		990.7	1036.1	1		750.0	786.7	2		987.4	1032.5	1
A″ CH_2 wag		914.9	954.9	23		714.1	743.2	11		904.7	944.4	23
A′ HCCH IP s. bend	882.1	871.0	913.3	27		632.3	663.2	13	880.8	868.7	910.8	27
A′ C−La str.	469	452.7	456.4	113		410.3	413.7	88	455	440.5	444.2	109
A″ CH_2 twist		333.6	349.0	37		250.1	261.5	22		331.8	347.2	36
A′ CLaH bend		291.3	291.4	99		218.9	219.2	36		290.5	290.4	99
A′ CCLa bend		212.3	204.2	33		183.5	176.5	38		206.9	199.1	31
A″ LaH OOP bend		31.1	113.0	73		20.4	77.4	34		34.1	113.5	74

[a] Frequencies and intensities are in cm^{-1} and km/mol, respectively. [b] Observed in an argon matrix. [c] Frequencies computed with BPW91/6-311++G(3df,3pd). [d] Frequencies and intensities computed with B3LYP/6-311++G(3df,3pd). SDD core potential and basis set are used for La. $HLa-CHCH_2$ has a planar structure.

TABLE 9: Calculated Frequencies of the Fundamental Bands of $H_2La-C_2H_2$ in Its Ground $^2A'$ State[a]

	$H_2La-C_2H_2$			$D_2La-C_2D_2$			$H_2La-^{13}C_2H_2$			HDLa−CHCD		
description	BPW91[b]	B3LYP[c]	int.[c]	BPW91[b]	B3LYP[c]	int.[c]	BPW91[b]	B3LYP[c]	int[c]	BPW91[b]	B3LYP[c]	int[c]
A_1 C−H str.	3156.8	3215.9	0	2431.5	2476.6	9	3140.4	3199.2	1	3130.9	3189.6	0
B_2 C−H str.	3101.5	3159.8	0	2272.8	2315.5	0	3092.8	3150.9	0	2356.2	2400.3	6
A_1 C═C str.	1730.5	1767.1	51	1605.8	1640.1	43	1669.9	1705.2	46	1662.4	1697.7	45
A_1 LaH_2 s. str.	1335.7	1323.7	622	946.4	938.0	316	1335.6	1323.7	622	929.7	916.5	515
B_1 LaH_2 as. str.	1284.2	1260.5	1222	913.8	896.9	624	1284.2	1260.5	1222	1310.7	1293.5	880
A_1 HCCH IP s. bend	732.4	747.2	19	538.7	548.8	2	730.4	745.2	21	690.3	712.2	78
A_2 HCCH OOP as.bend	682.2	717.5	0	560.7	589.1	0	672.9	707.8	0	645.3	677.2	15
B_2 HCCH IP as. bend	636.9	672.5	169	506.9	534.9	99	630.9	666.1	167	517.9	540.2	66
B_1 HCCH OOP s. bend	545.4	564.3	100	409.2	423.2	55	542.9	561.7	96	470.9	473.7	116
A_1 LaH_2 scis.	530.8	526.4	242	385.8	384.3	148	530.4	526.0	240	452.2	462.4	139
A_1 LaC_2 s. str.	316.7	317.1	13	296.3	295.9	2	307.2	307.7	13	311.2	312.1	11
B_2 LaC_2 as. str.	281.8	291.5	20	257.6	266.2	17	272.9	282.3	19	267.3	276.0	20
B_1 LaH_2 rock	260.2	258.1	41	188.3	187.0	19	259.9	257.8	42	211.8	210.2	25
A_2 LaH_2 twist	53.6	134.4	0	49.1	102.5	0	51.5	133.2	0	52.0	117.1	8
B_2 LaH_2 wag	158.8	130.0	569	113.6	93.5	292	158.7	129.9	569	138.7	111.3	423

[a] Frequencies and intensities are in cm^{-1} and km/mol, respectively. [b] Frequencies computed with BPW91/6-311++G(3df,3pd). [c] Frequencies and intensities computed with B3LYP/6-311++G(3df, 3pd). SDD core potential and basis set are used for La. $H_2La-C_2H_2$ has a C_{2v} structure.

reveal that H_2-elimination of ethylene becomes faster with going down the family column. The identified primary products correlate with the relative DFT energies of the products in the proposed reaction path in the doublet potential energy surface. The present and previous results demonstrate that C−H insertion and subsequent rearrangement readily occur with Groups 3−6 early transition metals and even actinides.[10–14] The DFT results also show that unlike the previously studied systems, the C−M and C−C bonds of the Group 3 metal dihydrido cyclic complexes are the longest and shortest among those of the plausible products. The weak C−M and strong C−C bonds indicate that the most electron-deficient transition metals lead to a weak C−M bond and insignificant back-donation to the triangular π-system.

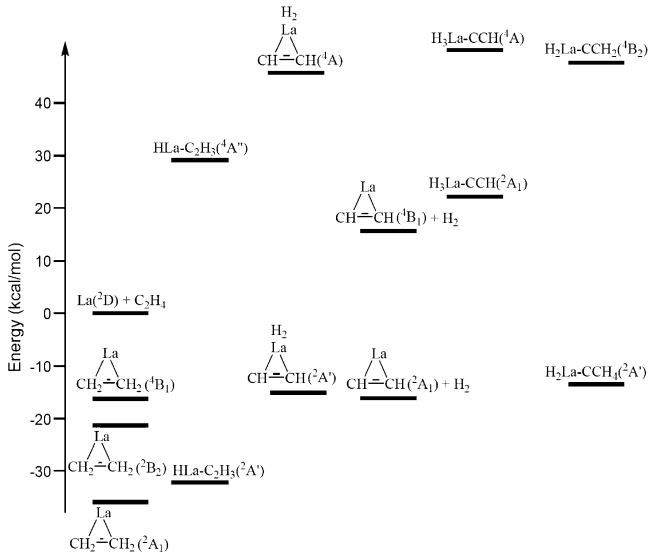

Figure 11. The energies of the plausible products relative to the reactants (La(^{2}D) + ethylene). Notice that the metallacyclopropane and insertion complexes in the doublet ground states are the most stable products, and the dihydrido cyclic complex is much higher in energy. Only the insertion product is identified from the matrix IR spectra (see text). The H_2-elimination product (La−C_2H_2($^2A_1$) + H_2) is 16.6 kcal/mol lower than the reactants, and many LaH_x absorptions are observed, including the strong LaH_4^- absorption.

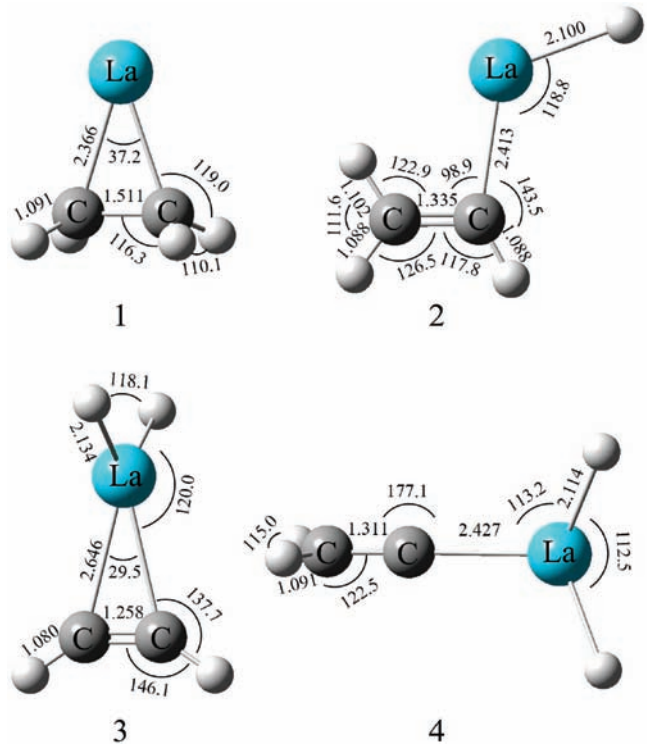

Figure 12. The B3LYP structures of the most plausible products from reaction of La atoms with ethylene. The metallacyclopropane (1) has a C_{2v} structure, the insertion product (2) a planar C_s structure, the dihydrido cyclic complex (3) a C_2 structure, and the vinylidene complexes (4) an allene-type C_s structure. The illustrated structures are for the doublet ground states.

Acknowledgment. We gratefully acknowledge financial support from National Science Foundation (U.S.) Grant CHE 03-52487 to L.A. and support from Korea Institute of Science and Technology Information (KISTI) by Grant No. KSC-2008-S02-0001.

Supporting Information Available: Tables S1, S2, and S3 of calculated unobserved metallacyclopropane product frequencies. This material is available free of charge via the Internet at http://pubs.acs.org.

References and Notes

(1) (a) Yi, S. S.; Blomberg, M. R. A.; Siegbahn, P. E. M.; Weisshaar, J. C. *J. Phys. Chem. A* **1998**, 102. (b) Reichert, E. L.; Yi, S. S.; Weisshaar, J. C. *Int. J. Mass Spectrom.* **2000**, *196*, 55. (c) Wen, Y.; Poremski, M.; Ferrett, T. A.; Weisshaar, J. C. *J. Phys. Chem. A* **1998**, *102*, 8362. (d) Carroll, J. J.; Haug, K. L.; Weisshaar, J. C. *J. Am. Chem. Soc.* **1993**, *115*, 6962. (e) Poremski, M.; Weisshaar, J. C. *J. Phys. Chem. A* **2000**, *104*, 1524 (Zr + hydrocarbons).

(2) (a) Schroden, J. J.; Wang, C. C.; Davis, H. F. *J. Phys. Chem. A* **2003**, *107*, 9295. (b) Porembski, M.; Weisshaar, J. C. *J. Phys. Chem. A* **2001**, *105*, 6655. (c) Hinrichs, R. Z.; Schroden, J. J.; Davis, H. F. *J. Phys. Chem. A* **2003**, *107*, 9284 (Y + hydrocarbons). (d) Willis, P. A.; Stauffer, H. U.; Hinrichs, R. Z.; Davis, H. F. *J. Phys. Chem. A* **1999**, *103*, 3706.

(3) (a) Siegbahn, P. E. M.; Blomberg, M. R. A.; Svensson, M. *J. Am. Chem. Soc.* **1993**, *115*, 1952. (b) Blomberg, M. R. A.; Siegbahn, P. E. M.; Svensson, M. *J. Phys. Chem.* **1992**, *96*, 9794. (c) Blomberg, M. R. A.; Siegbahn, P. E. M.; Yi, S. S.; Noll, R. J.; Weisshaar, J. C. *J. Phys. Chem. A* **1999**, *103*, 7254. (d) Rivalta, I.; Russo, N.; Sicilia, E. *J. Mol. Struct.: THEOCHEM* **2006**, *762*, 25.

(4) (a) Carroll, J. J.; Haug, K. L.; Weisshaar, J. C.; Blomberg, M. R. A.; Siegbahn, P. E. M.; Svensson, M. *J. Phys. Chem.* **1995**, *99*, 13955. (b) Carroll, J. J.; Weisshaar, J. C. *J. Phys. Chem.* **1996**, *100*, 12355. (c) Poremski, M.; Weisshaar, J. C. *J. Phys. Chem. A* **2001**, *105*, 4851 (Zr + C_2H_4 reaction path).

(5) (a) Stauffer, H. U.; Hinrichs, R. Z.; Schroden, J. J.; Davis, H. F. *J. Phys. Chem. A* **2000**, *104*, 1107. (b) Poremski, M.; Weisshaar, J. C. *J. Phys. Chem. A* **2001**, *105*, 6655 (Y + C_2H_4). (c) Hinrichs, R. Z.; Schroden, J. J.; Davis, H. F. *J. Am. Chem. Soc.* **2003**, *125*, 860.

(6) Andrews, L.; Cho, H.-G. *Organometallics* **2006**, *25*, 4040, and references therein (Review article).

(7) (a) Davies, H. M.; Beckwith, R. E. J. *Chem. Rev.* **2003**, *103*, 2861. (b) Hall, C.; Perutz, R. N. *Chem. Rev.* **1996**, *96*, 3125. (c) Campos, K. R. *Chem. Soc. Rev.* **2007**, *36*, 1069.

(8) (a) Proctor, D. L.; Davis, H. F. *Proc. Natl. Acad. Sci. U.S.A.* **2008**, *105*, 12677. (b) Davis, S. C.; Klabunde, K. J. *J. Am. Chem. Soc.* **1978**, *100*, 5973. (c) Billups, W. E.; Konarski, M. M.; Hauge, R. H.; Margrave, J. L. *J. Am. Chem. Soc.* **1980**, *102*, 7393.

(9) (a) Olson, D. E.; Bois, J. Du. *J. Am. Chem. Soc.* **2008**, *130*, 11248. (b) Shilov, A. E.; Shul'pin, G. B. *Chem. Rev.* **1997**, *97*, 2879.

(10) Lee, Y. K.; Manceron, L.; Papai, I. *J. Phys. Chem. A* **1997**, *101*, 9650.

(11) (a) Cho, H.-G.; Andrews, L. *J. Phys. Chem. A* **2004**, *108*, 3965 (Zr + C_2H_4). (b) Cho, H.-G.; Andrews, L. *J. Phys. Chem. A* **2004**, *108*, 10441 (Ti and Hf + C_2H_4).

(12) Cho, H.-G.; Andrews, L. *J. Phys. Chem. A* **2007**, *111*, 5201 (Group 5 + C_2H_4).

(13) Cho, H.-G.; Andrews, L. *J. Phys. Chem. A* **2008**, *112*, 12071 (Group 6 + C_2H_4).

(14) Cho, H.-G.; Andrews, L. *J. Phys. Chem. A* **2009**, *113*, 5073 (Th, U + C_2H_4).

(15) (a) Andrews, L.; Citra, A. *Chem. Rev.* **2002**, *102*, 885, and references therein. (b) Andrews, L. *Chem. Soc. Rev.* **2004**, *33*, 123, and references therein.

(16) Frisch, M. J.; Trucks, G. W.; Schlegel, H. B.; Scuseria, G. E.; Robb, M. A.; Cheeseman, J. R.; Montgomery, J. A., Jr.; Vreven, T.; Kudin, K. N.; Burant, J. C.; Millam, J. M.; Iyengar, S. S.; Tomasi, J.; Barone, V.; Mennucci, B.; Cossi, M.; Scalmani, G.; Rega, N.; Petersson, G. A.; Nakatsuji, H.; Hada, M.; Ehara, M.; Toyota, K.; Fukuda, R.; Hasegawa, J.; Ishida, M.; Nakajima, T.; Honda, Y.; Kitao, O.; Nakai, H.; Klene, M.; Li, X.; Knox, J. E.; Hratchian, H. P.; Cross, J. B.; Bakken, V.; Adamo, C.; Jaramillo, J.; Gomperts, R.; Stratmann, R. E.; Yazyev, O.; Austin, A. J.; Cammi, R.; Pomelli, C.; Ochterski, J. W.; Ayala, P. Y.; Morokuma, K.; Voth, G. A.; Salvador, P.; Dannenberg, J. J.; Zakrzewski, V. G.; Dapprich, S.; Daniels, A. D.; Strain, M. C.; Farkas, O.; Malick, D. K.; Rabuck, A. D.; Raghavachari, K.; Foresman, J. B.; Ortiz, J. V.; Cui, Q.; Baboul, A. G.; Clifford, S.; Cioslowski, J.; Stefanov, B. B.; Liu, G.; Liashenko, A.; Piskorz, P.; Komaromi, I.; Martin, R. L.; Fox, D. J.; Keith, T.; Al-Laham, M. A.; Peng, C. Y.; Nanayakkara, A.; Challacombe, M.; Gill, P. M. W.; Johnson, B.; Chen, W.; Wong, M. W.; Gonzalez, C.; Pople, J. A. *Gaussian 03*, revision C.02; Gaussian, Inc.: Wallingford, CT, 2004.

(17) (a) Becke, A. D. *J. Chem. Phys.* **1993**, *98*, 5648. (b) Lee, C.; Yang, Y.; Parr, R. G. *Phys. Rev. B* **1988**, *37*, 785.

(18) Raghavachari, K.; Trucks, G. W. *J. Chem. Phys.* **1989**, *91*, 1062.

(19) Cao, X. Y.; Dolg, M. *J. Mol. Struct.: THEOCHEM* **2002**, *581*, 139.

(20) Burke, K.; Perdew, J. P.; Wang, Y. In *Electronic Density Functional Theory: Recent Progress and New Directions*; Dobson, J. F., Vignale, G., Das, M. P., Eds.; Plenum: New York, 1998.

(21) (a) Scott, A. P.; Radom, L. *J. Phys. Chem.* **1996**, *100*, 16502. (b) Andersson, M. P.; Uvdal, P. L. *J. Phys. Chem. A* **2005**, *109*, 3937.

(22) (a) Wang, X.; Chertihin, G. V.; Andrews, L. *J. Phys. Chem. A* **2002**, *106*, 9213. (b) Wang, X.; Andrews, L. *J. Am. Chem. Soc.* **2002**, *124*, 7610 (Sc, Y, and La + H_2).

(23) Chertihin, G. V.; Andrews, L.; Bauschlicher, C. W., Jr. *J. Am. Chem. Soc.* **1998**, *120*, 3205 (cyc-$(ScN)_2$).

(24) Chertihin, G. V.; Bare, W. D.; Andrews, L. *J. Phys. Chem. A* **1998**, *102*, 3697 (cyc-$(LaN)_2$).

(25) Andrews, L.; Zhou, M.; Chertihin, G. V.; Bauschlicher, C. W., Jr. *J. Phys. Chem. A* **1999**, *103*, 6525 ($OLaO^-$).

JP9025464